Supporting information

Gate-tunable Giant Stark Effect in Few-layer Black Phosphorus

Yanpeng Liu[1,2,Υ], Zhizhan Qiu[1,3,Υ], Alexandra Carvalho[2,4,Υ], Yang Bao[1,2], Hai Xu[1,2], Sherman J. R. Tan[1,3], Wei Liu[1,2], A. H. Castro Neto[2,4], Kian Ping Loh[1,2,*] and Jiong Lu[1,2,*]

[1]Department of Chemistry, National University of Singapore, 3 Science Drive 3, Singapore 117543

[2]Centre for Advanced 2D Materials and Graphene Research Centre, National University of Singapore, Singapore 117546

[3]NUS Graduate School for Integrative Sciences and Engineering, National University of Singapore, 28 Medical Drive, Singapore 117456

[4]Department of Physics, National University of Singapore, 3 Science Drive 2, Singapore 117542

  *Email: chmlohkp@nus.edu.sg (K.P.L.); chmluj@nus.edu.sg (J.L.)

Table of Contents

1. Methods and materials

Sample fabrication. The exfoliation of BP was carried out in a glove box filled with argon gas (O_2 and H_2O < 0.5 ppm). Typically, a thin BP flake was directly mechanically exfoliated from a bulk BP crystal (HQ graphene) onto a PDMS (Polydimethylsiloxane) substrate using blue "magic" tape. The desired BP flake was then identified using optical microscopy and transferred onto a Si/SiO_2 substrate patterned with a gold pad (a gold pad with dimension ~ 400×400 μm^2 and 50 nm thick was previously deposited) with a dry transfer method via a home-built transfer platform under argon in a glove box.[37] During STM measurements, one corner of the BP flake sits on top of the gold pad and the rest is on the Si/SiO_2 substrate. The wiring between the gate electrode and the sample is made of aluminum wire. After wire bonding, the BP sample was annealed at 220℃ in the preparation chamber (<10^{-10} torr) to remove possible absorbents and to achieve a better contact. The overall air-exposure duration of device is less than 2 min to minimize the surface degradation of BP flakes.[33-36]

STM and STS measurements. The measurements were performed using Omicron ultrahigh-vacuum LT-STM (<10^{-11} torr). The tungsten tip was calibrated by verifying the surface state of the Au (111) crystal. All the STM images were captured in constant-current mode at LN_2 and LHe temperatures (details are provided in the main text). STS data were acquired using the external lock-in technique (SR830 Lock-In Amplifier, bias modulations of 5-10 mV at 773.1 Hz).

Theoretical calculations. First-principles calculations based on density-functional theory were used to compute the electronic structure of few-layer phosphorene. The calculations were performed using the Quantum ESPRESSO code.[53] The core electrons were treated using a Troulier-Martins pseudopotential.[54] The Kohn-Sham orbitals were expanded in a plane-wave basis with a cut-off energy of 50 Ry. The exchange and correlation interactions were described using the PBE functional, and additional hybrid functional calculations were performed using the HSE functional.[55,56] The electric field was applied in the form of a saw-tooth potential along the direction perpendicular to the layer.

2. Layer number determination of measured thin BP flake

The thickness of the BP flake was determined using a Dimension FastScan Bruker AFM. Since the average thickness of monolayer BP is ~0.55 nm, the layer number of BP flake is identified to be 11, and this is further confirmed using the optical contrast method.[14]
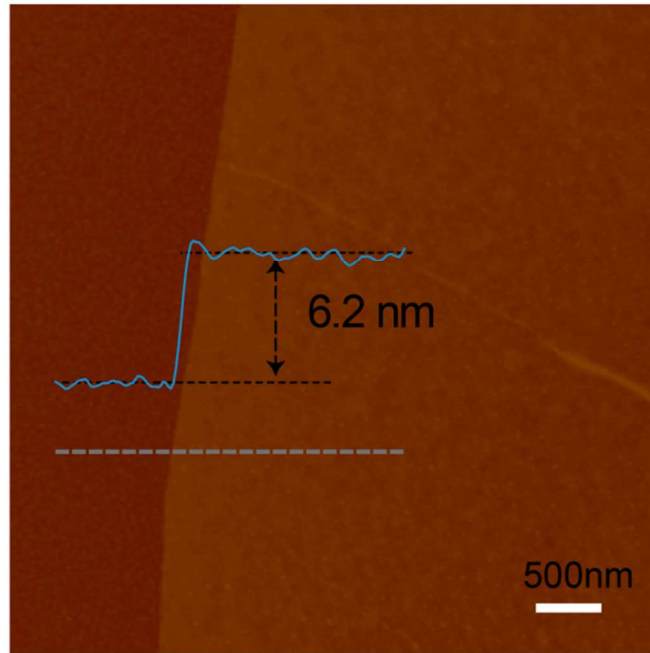

Figure S1. AFM image of few-layers BP on a silicon wafer.

3. Bandgap determination method of few-layer BP flake

Based on the statistical analysis of 52 STS curves, the electronic bandgap (E_g) of non-gated BP sample was determined to be 0.31 ± 0.02 eV, where 0.31 is the mean value and 0.02 is the standard derivation of the mean.

For each STS curve, we follow a procedure described previously to determine the VBM, CBM and E_g.[41] First, we offset all data vertically by a factor of 2 times the absolute value of the overall minimum value of the spectrum. This treatment makes all value of signal positive while retaining all the features presented in the original STS curve. After that, the curves were converted into logarithmic scale. A horizontal line $C_{g,av}$ (given by the logarithm of the mean value of the signal within the gap) is drawn through spectra. Using linear fittings of the CB and VB band near the edge, the E_{VBM} and E_{CBM} are determined at the intersection of the lines as illustrated in Fig. S2 below. Therefore, the electronic bandgap can be calculated using this equation: $E_g = E_{CBM} - E_{VBM}$.
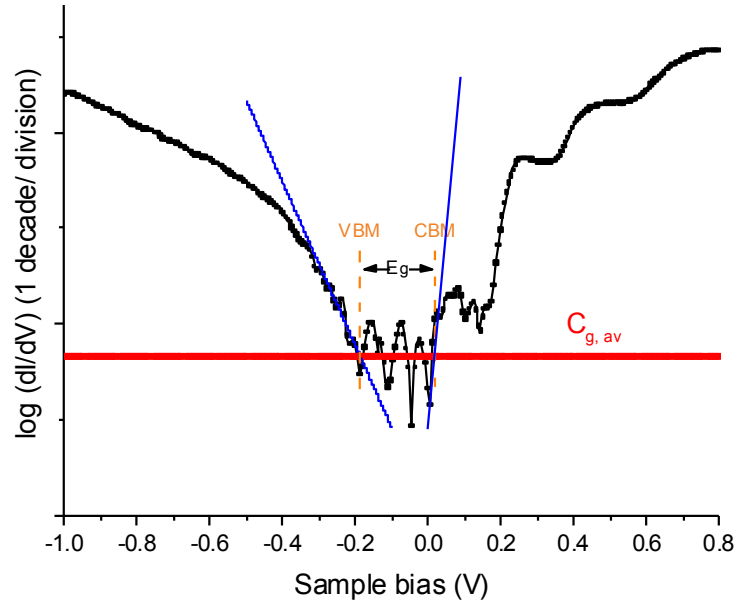
Figure S2. Sample of determination of VBM, CBM and E_g from STS curve ($V_g = +50V$). The red horizontal line $C_{g,av}$ is the logarithm format of the mean value of signals within the bandgap. The blue line is the linear fit of CB and VB near the edges. VBM and CBM are given by the intersection of red and blue lines.

3

4. Electric properties of BP with different layer number as function of electric field

As predicted in Fig. S3a, the magnitude and slope of bandgap modulation by the Stark effect vary with the layer number of BP and the slope (dE_g/dE_{ext}) increases monotonically as a function of layer thickness. Consequently, we can see that the Stark coefficient (Fig. S3b) is larger for thicker BP samples.
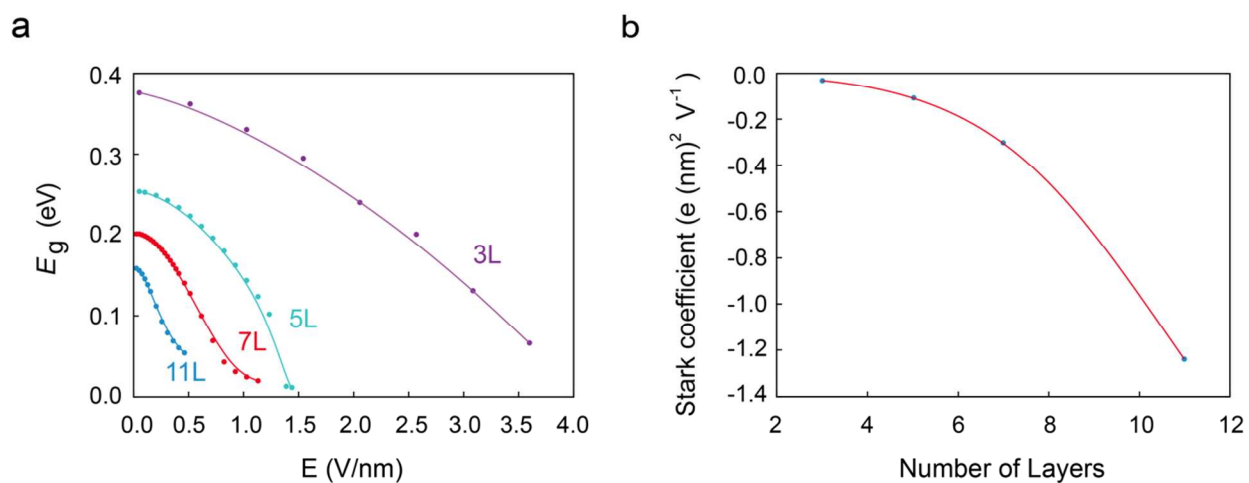
Figure S3. Simulated electronic properties of BP under electric fields. (a), Bandgap reduction of BP with various thickness *vs* external electric field. (b) Layer-number dependence of BP Stark coefficient.

5. Quantum capacitance model of gated BP sample
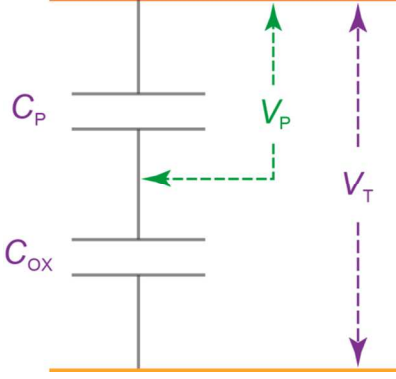
Figure S4. Schematic illustration of double layer capacitors from series connection of C_P and C_{OX}. C_P represents the quantum capacitance of BP while C_{OX} is the capacitance of silicon dioxide layer.

For two planar capacitors in series shown in Fig. S4:

$$\frac{1}{C_T} = \frac{1}{C_P} + \frac{1}{C_{ox}} \tag{1}$$

$$C = \frac{Q}{V} \tag{2}$$

$$Q = C_T * V_T = C_P * V_P \tag{3}$$

$$V_P = V_T * \frac{C_T}{C_P} = V_T * \frac{C_{ox}}{C_P + C_{ox}} \tag{4}$$

Where $C = (\varepsilon * A)/(4\pi * d)$, d is the thickness; A represents the working area; ε is the dielectric constant. For SiO$_2$, $\varepsilon_{ox} = 3.9$ and $\varepsilon_{P,\perp} = 8.3$ for phosphorene.

Finally, we could obtain:

$$E = \frac{V_P}{d_P} = \frac{V_T * \varepsilon_{ox}}{d_P * \varepsilon_{ox} + d_{ox} * \varepsilon_P}$$

6.   Other possible origin of resonance feature in STS spectra

Many-body excitations were reported to renormalize the band structure of 2D materials.[44,46,47] This effect in turn introduces additional resonance features in the tunneling spectra arising from many-body interactions such as electron-phonon and electron-plasmon coupling. However, the energy separation of adjacent resonances observed here is larger than 100 meV, much higher than the most energetic of phonon modes of BP (~ 66.1 meV).[38] Electron-plasmon coupling often induces broad and weak features in dI/dV spectra owing to the coupling between plasmon and electron-hole excitation in a wide energy window. In addition, the features induced by electron-plasmon coupled should be carrier-concentration dependent. The observation of a nearly-rigid shift of resonance peaks together with the band edges rule out the possible contribution of electron-plasmon coupling. Moreover, we also have considered the possible origin of the resonance features arising from the quantum confinement.[48] The energy gap between quantum confined states is expected to vary monotonically as function of energy levels with different quantum numbers, in contrast to the trend we observed here for the energy separations between resonance features (the peak-to-peak separations first increase and then decrease with increasing energy).

7. Tip-induced band bending: Bandgap of BP flake as a function of tip-sample separation

The effect of tip-induced band bending (TIBB) may complicate the bandgap determination of semiconducting BP using STS.[41] The unscreened electric fields induced by biased tip may shift the VBM and CBM, and thus cause the variation in the measured bandgap. In this work, we verify that the TIBB effect does not have a significant role in our study by varying the tip-sample distances for STS measurement.

The range of set point current for the dI/dV spectra shown in Fig. S5a corresponds to a total variation of tip-sample distance of ~0.67±0.04 Å.[24,41] As shown in Fig. S5b, the total variation of measured bandgap is ~20 meV (ΔE_{CBM}= + 10 meV, ΔE_{VBM}= − 10 meV) when the tip-sample decreases in this tip-sample distance range. The slight variation (6.45% of the bandgap of few-layer BP) indicates that TIBB does not have a significant role and could be ruled out as an origin of bandgap reduction.
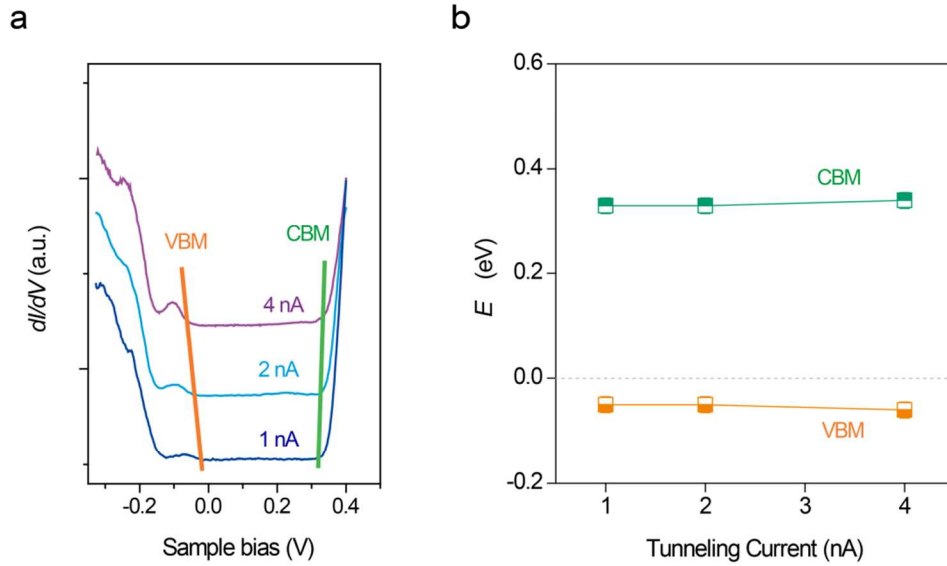

Figure S5. Tip height-dependent STS data (a) and band structure variation as function of tunneling current (b). The STS were collected at non-defective region of BP flake.
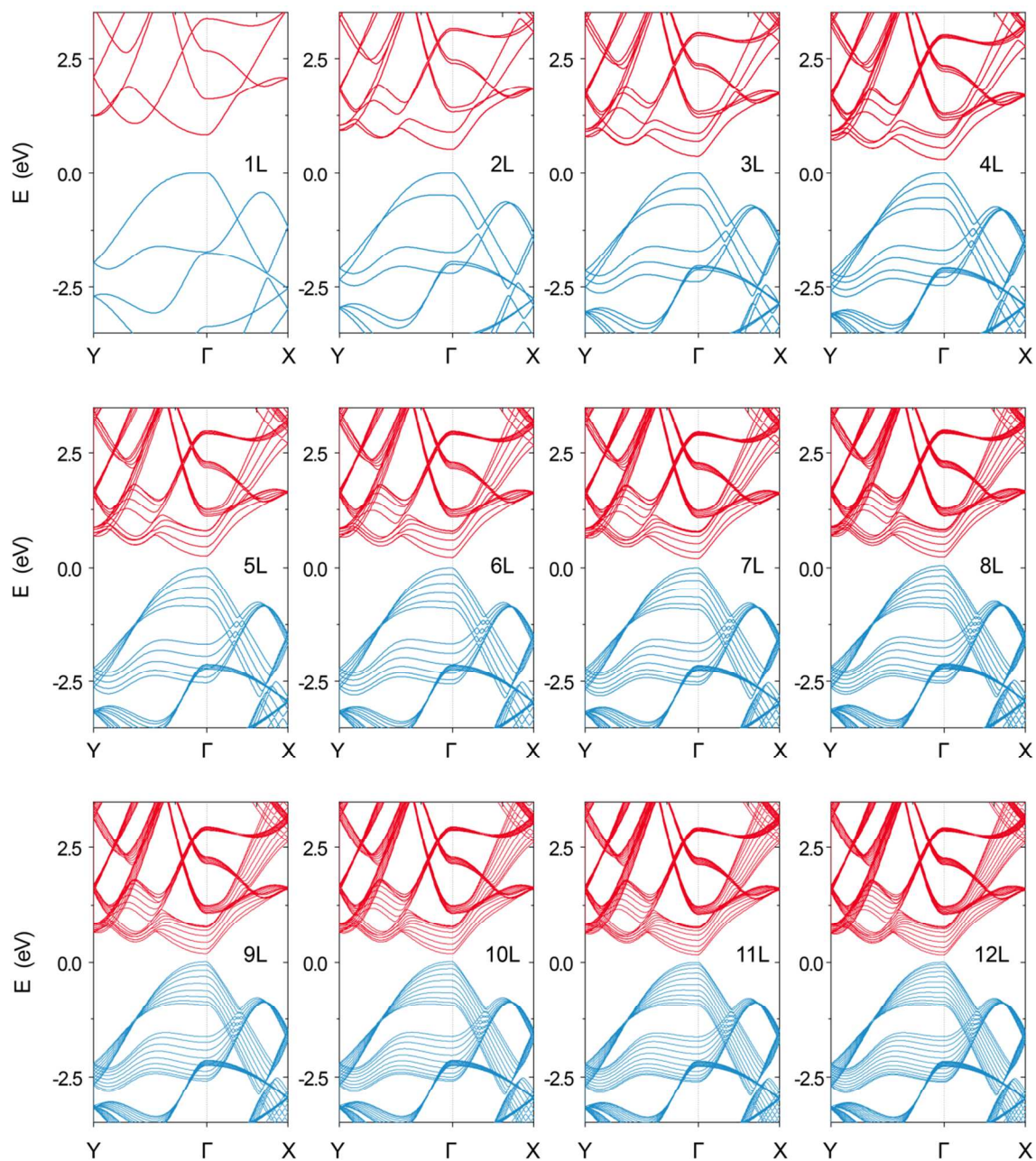
8. Layer dependent sub-bands structure of few-layer BP sample

Sub-bands structure of BP sample is determined to be layer-dependent mentioned in the main text. To further verify this model, we preformed local STM spectroscopy measurement on a 7-layer and 11-layer BP flake respectively as shown in Fig. S6. It is clear that the observed feature positions in STS spectra could be predicted very well by p-LDOSs from DFT calculations for both 7-layer and 11-layer BP devices. The peak-to-peak interval of 7-layer BP increase faster (with respect to the Fermi energy) than that of 11-layer before the value of peak-to-peak interval converges a maximum, which is in good agreement with the tight binding model (Fig. 4d). For 7-layer BP, the peak-to-peak interval follows the estimated $(E_{N,n} - E_{N,n}^0)/2$ value and the maximum peak-to-peak interval reaches ~0.20eV ($|E_{V3} - E_{V2}|$, calculated value is ~0.19eV). For 11-layer BP, the same trend occurs but the maximum peak-to-peak interval reaches ~0.17eV ($|E_{V5} - E_{V4}|$). Therefore, STS evaluation of the sub-bands structure can serve as a characterization tool to determine the layer number accurately.[16]
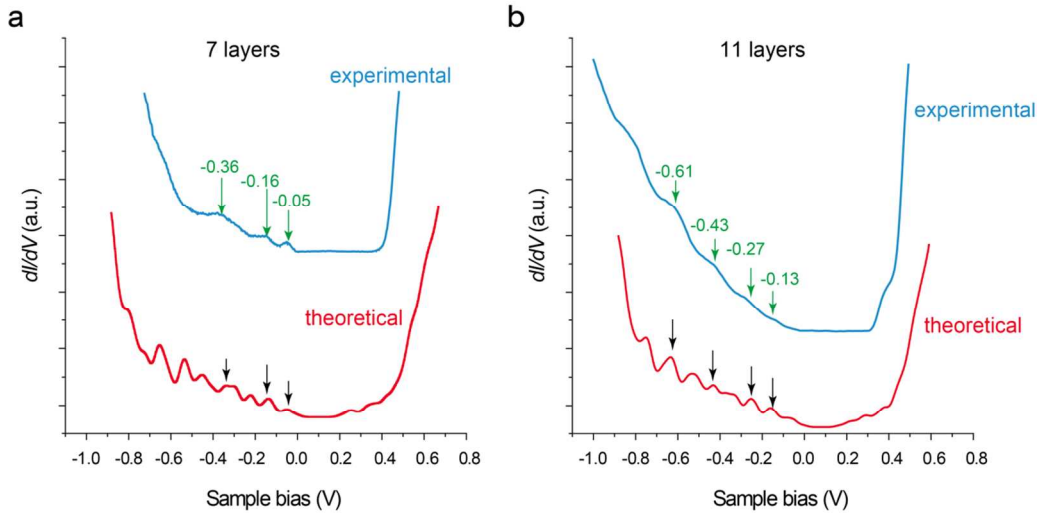
Figure S6. Experimental and theoretical layer-dependent STS spectra of few-layer BP (a, 7 layers; b, 11 layers). For 7-layer BP, Calculated peak energy positions (marked with arrows in (a), red line) are: E_{V1}=-0.05eV, E_{V2}=-0.14eV, and E_{V3}=-0.34eV, respectively. For p-DOS curve of 11-layer BP in (b), these peaks location are: E_{V2}=-0.15eV, E_{V3}=-0.26eV, E_{V4}=-0.43eV and E_{V5}=-0.62eV, respectively. E_{VBM} are -0.02eV both for 7-layer and 11-layer BP device. Here, the V_1 peak arising from the first sub-bands under VBM for 11-layer BP sample is very weak as it is too close to VBM. The zero of the energy scale is set to the top of the valence band.

9. Band structure calculations of 1-12 layer BP sample

Figure S7. Layer-dependent calculated band structure of few-layer BP (1-12 layers). The zero of the energy scale is set to the top of the valence band. It can be seen very clearly that the valence and conduction band split into N sub-bands where N = number of layers in BP.

References

53. Giannozzi, P.; Baroni, S.; Bonini, N.; Calandra, M.; Car, R.; Cavazzoni, C.; Ceresoli, D.; Chiarotti, G.L.; Cococcioni, M.; Dabo, I.; Dal Corso, A. *J. Phys. Condens. Matter.* **2009**, *21*, 395502.

54. Troullier, N.; Martins, J. L. *Phys. Rev. B.* **1991**, *43*, 1993.

55. Perdew, J. P.; Burke, K.; Ernzerhof, M. *Phys. Rev. Lett.* **1996**, *77*, 3865–3868.

56. Heyd, J.; Scuseria, G. E.; Ernzerhof, M. *J. Chem. Phys.* **2006**, *124*, 219906.